2016

Textile Al2O3–TiO2 nanocomposite as an antimicrobial and radical scavenger wound dressing

Shokoh Parham, *University Technology Malaysia*
Sheela Chandren, *University Technology Malaysia*
Dedy H.B. Wicaksono, *University Technology Malaysia*
Saeedeh Bagherbaigi, *University Technology Malaysia*
Siew Ling Lee, *University Technology Malaysia*, et al.

RSC Advances

PAPER

Cite this: *RSC Adv.*, 2016, **6**, 8188

Textile/Al_2O_3–TiO_2 nanocomposite as an antimicrobial and radical scavenger wound dressing

Shokoh Parham,[a] Sheela Chandren,[a] Dedy H. B. Wicaksono,[bc] Saeedeh Bagherbaigi,[b] Siew Ling Lee,[a] Lai Sin Yuan[a] and Hadi Nur*[a]

Received 1st October 2015
Accepted 10th January 2016

DOI: 10.1039/c5ra20361a

www.rsc.org/advances

Improving the antimicrobial activity and radical scavenging ability of a textile-based nanocomposite (textile/TiO_2, textile/Al_2O_3/TiO_2, textile/Al_2O_3 and textile/Al_2O_3–TiO_2 bimetal oxide nanocomposite) is the key issue in developing a good and flexible wound dressing. In this work, flexible textile attached with Al_2O_3–TiO_2 nanoparticles was prepared by dipping the textile in a suspension containing Al_2O_3–TiO_2 nanoparticles (150 mmol l^{-1}). The mean radical scavenging ability for textile/TiO_2, textile/Al_2O_3/TiO_2, textile/Al_2O_3 and textile/Al_2O_3–TiO_2 bimetal oxide nanocomposites as measured by liquid ultraviolet visible spectroscopy (UV-Vis) coupled with dependence formula was 0.2%, 35.5%, 35.0% and 38.2%, respectively. Based on the X-ray diffraction (XRD) patterns, the preface reactive oxygen species (ROS) scavenging ability shown by the textile/Al_2O_3–TiO_2 bimetal oxide nanocomposite is most probably caused by the crystal structure concluding in a corundum-like structure, with Al^{3+} ions filling the octahedral sites in the lattice. Increased antimicrobial activity measured by optical density at 600 nm recorded for textile/Al_2O_3–TiO_2 bimetal oxide nanocomposites showed better interaction between Al_2O_3 and TiO_2 nanoparticles. This good interaction is expected to lead to better antimicrobial and radical scavenging ability as shown by the *E. coli* and human skin fibroblast (HSF) cytotoxicity tests, respectively.

1. Introduction

Wound dressings are usually designed to be in direct contact with the wound, in order to prevent further harm and support healing. The main difference between wound dressings and bandages is that bandages are mainly used to hold a wound dressing in place while wound dressings contribute to the healing process. Many types of wound dressing already exist on the market, such as fabric, spider webs, manure, leaves and honey.[1] Currently, the most commonly used wound dressing materials are gauze, films, gels, foams, hydrocolloids, alginates, hydrogels, polysaccharide beads, pasta and granules.[2] In wound dressing materials, a layer of non-sticking film over the absorbent material is added in order to prevent direct adhesion to the wound.[3]

Parallel to immediate improvement of wound dressings, control of a microorganism's harmful effects would be necessary.[4] A broad range of microorganisms can coexist in natural equilibrium with the human body and living environments. This uncontrolled fast thriving of microbes can lead to some serious problems, such as dangerously infected wounds.[4]

Recently, the use of nanoparticles in clinical and experimental settings has increased due to their wide range of biomedical applications, for example in wound healing, imaging and drug delivery. The antimicrobial ability and non-toxicity are two key factors for biomedical applications like wound healing. In this context, it is widely accepted that cytotoxicity to human or animal cells depends on some parameters such as mechanism of antimicrobial action. However, recent literature suggests that cytotoxicity of some nanoparticles such as TiO_2, Ag and ZnO is related to oxidative stress. This toxicity is related to the generation of reactive oxygen species (ROS) free radicals. Previous researchers also reported that the toxicity of Al_2O_3 is not high because of its role as radical scavenger. Therefore it can block ROS generation.[5,6]

Generally, antimicrobial agents are used to prevent the harmful effects of microorganisms. Most of the existing wound dressing uses textile.[8] Antimicrobial agents are attached on textiles to prevent the undesirable effects of textiles, such as the degradation phenomena of staining, deterioration and coloring of fibers.[7] Due to their dye degradation potential, even some fungus can be used to remove dyes,[8] unpleasant odors,[9] and decrease the potential health risks of textiles.[10]

[a]*Centre for Sustainable Nanomaterials, Ibnu Sina Institute for Scientific and Industrial Research, Universiti Teknologi Malaysia, 81310 UTM Skudai, Johor, Malaysia. E-mail: hadi@kimia.fs.utm.my*

[b]*Medical Devices and Technology Research Group (MediTeg), Faculty of Biosciences and Medical Engineering, Universiti Teknologi Malaysia, 81310 UTM Skudai, Johor, Malaysia*

[c]*IJN-UTM Cardiovascular Engineering Centre, Faculty of Biosciences and Medical Engineering, Universiti Teknologi Malaysia, 81310 UTM Skudai, Johor, Malaysia*

Conventional textile wound dressings, however, do not possess any resistance towards microorganisms and materials generated from their metabolism.[4] They are most commonly prone to multiplication, proliferation and accumulation of microorganisms into their surrounding environment.[11] In fact, several factors such as temperature, humidity and presence of materials on the textile's surfaces can make the textile an optimal enrichment culture for a rapid multiplication of microorganisms.[12] Therefore, the control of these terrible effects is necessary.

Based on the above reasons, the high antimicrobial property of textile wound dressings is necessary. This can be achieved by, the use of metal oxide nanoparticles such as titania (TiO_2) and silver oxide (AgO), as they are known to possess strong antimicrobial properties.[13] Apart from these metal oxides, alumina (Al_2O_3) nanoparticles have wide-range applications in industries, however, Al_2O_3 lacks strong antimicrobial activity.[23] When metal oxide is a base for mixed oxide, therefore mixed oxide may be able to be used as antimicrobial agents. Zirconia (ZrO_2), Al_2O_3, silica (SiO_2) and TiO_2 are some of the base for making mixed metal oxide supports. Different kinds of mixed metal oxides have been reported such as ZrO_2–TiO_2, TiO_2–SiO_2 and Al_2O_3–SiO_2.[14]

Currently, nanosized inorganic and organic nanoparticles are finding increasing applications in medical devices, *e.g.* as antimicrobial agents due to their ability to be biologically functionalized.[15] Antimicrobial agents have a lot of industrial applications in health care, medical care, synthetic textiles and environmental products.[16,17] Antibacterial activity is known to be a function of the surface area in contact with the microorganisms; therefore a larger surface area (as in the case of nanoparticles) shows a broader range of probable reactions with bioorganic present on the cell surface, such as environmental organic and inorganic species.[18] However, the antimicrobial activity of these nanoparticles can produce ROS free radicals, which are toxic to human cell. Previous studies on the toxicity of metal oxide nanoparticles to bacterial species are limited, even though their bactericidal properties have been reported in same biomedical literatures.[19]

Radical scavenging ability can decrease the toxicity of metal oxide to human cell. A scavenger is a chemical substance added to a mixture in order to deactivate or remove unwanted and impurities reaction products, such as oxygen, so as to avoid any unfavorable reactions.[20] Metal oxides are generally toxic to microbes in the environment.[19] It has been shown that nanoparticles with positive charge such as zinc oxide could bind the Gram-negative cell membrane by electrostatic attraction.[20] Clearly, the intimate relationship between the physicochemistry of the medium and membrane biology of the microbe is emerging as a key factor in nanoparticles toxicity to microorganisms.[21]

Only a few studies have been carried out on the interaction of the Al_2O_3 and Al_2O_3–TiO_2 bimetal oxide with microbes. One study found no detrimental effect of Al_2O_3 slurry between 62.5 and 250 mg l^{-1} concentration range on *E. coli*.[22] Past literatures have reported the toxicity and harmful effects of other antimicrobial agents.[23] The purpose of the current study is to improve the antimicrobial properties of textile as wound dressing without being toxic to human cell. This paper focuses on the synthesis and characterization of textile/Al_2O_3 nanocomposite, textile/TiO_2 nanocomposite textile/Al_2O_3/TiO_2 nanocomposite and textile/Al_2O_3–TiO_2 bimetal oxide nanocomposite as wound dressings. The antimicrobial properties and radical scavenging ability of these nanocomposites were also tested. The antimicrobial mechanism of these nanocomposites is also suggested.

2. Materials and methods

2.1. Reagents

The materials used in this study were citric acid ($C_6H_8O_7$–H_2O, QReC), aluminium nitrate ($Al(NO_3)_3$–$9H_2O$, QReC), sodium carbonate (Na_2CO_3, QReC), titanium isopropoxide ($C_{12}H_{28}O_4Ti$, Merck), ethyl acetoacetate ($C_6H_{10}O_3$, Merck), ethanol (C_2H_6O, Merck), hydrochloric acid (HCl, 96%, Merck), textile 100% cotton white plain weave cotton textile (Mirota Batik, Surabaya, Indonesia, unmercerized, bleached, having 126 denier, or 14 mg m^{-1} and a fabric count of 95 × 95, with a mass density of 9.3 mg cm^{-2}, and 160 fibers per inch), sodium hydroxide (NaOH 7 wt%, Merck) and sulfuric acid (H_2SO_4 96%, Merck). The bactericidal experiments were carried out with Gram-negative bacteria *Escherichia coli* (*E. coli*) (strain.DH5D-*E. coli*) in Luria Bertani (LB) medium (Himedia Laboratories Ltd). Tryptone or peptone (Sigma Aldrich), yeast extract (Sigma Aldrich), agar (Sigma Aldrich) were also used. The cytotoxicity test was carried out with human skin fibroblast (HSF 1184 catalogue no. 90011883, available from ECACC, United Kingdom). The minimum essential media (MEM) (catalogue no. 11095, Invitrogen), fetal bovine serum (FBS) (Sigma Aldrich), penicilin–streptomycin (PS) (Sigma Aldrich), PBS (phosphate buffered saline solutions) (Sigma Aldrich), trypsin/EDTA (Invitrogen), Hank's balanced salt solution (HBSS) (Sigma Aldrich) and ™Red CMTPX dye (Sigma Aldrich) were also used.

2.2. Textile preparation

Before the synthesis of the textile-based nanocomposite, the wax on the textile's surface was removed by sodium carbonate (Na_2CO_3). First, Na_2CO_3 (10 mg) and water as solvent (25 ml) was added to textile (1.5 g) in a beaker. The mixture was boiled for 5 min at 100 °C. After that, the mixture was washed with deionized water until the pH was 6–7 and then the sample was dried in air.[24] The weight of the textile used was 1.5 g.

2.3. Synthesis of textile/Al_2O_3 nanocomposite

The alumina nanoparticles were synthesized by using the sol–gel method. $Al(NO_3)_3 \cdot 9H_2O$ was added to citric acid. Then this mixture was dissolved in deionized water and stirred at 80 °C for 8 h. After that the yellowish residue was collected. The obtained sample was calcined in a furnace at 1100 °C for 2 h. The sample was then weighed and the data were collected.[25] The synthesis of textile/Al_2O_3 nanocomposite was done by functionalizing the prepared Al_2O_3 on textile. Textile (1.5 g) was soaked in a solution of Al_2O_3 nanoparticles (150 mmol l^{-1}), with NaOH solution (7 wt%) as the solvent. The solution was stirred for 24 h and then

immersed in a H_2SO_4 (5 wt%) water bath at 15 °C immediately for neutralization. After neutralization, the sample was washed with deionized water to remove the solvent. The sample was then dried in room temperature.

2.4. Synthesis of textile/TiO_2 nanocomposite

TiO_2 nanoparticle was also synthesis by using the sol–gel method. First, $C_{16}H_{36}O_4Ti$ (1 ml) and C_2H_5OH (5 ml) were added in a clean vial (10 ml). Then the solution was stirred at room temperature for 6 h. After that, deionized water (0.3 ml) and HCl (0.4 ml) were added before stirring the solution for 1 h. The obtained sample is dried in oven at 80 °C and then it was calcined at 800 °C for 2 h.[27] The synthesis of textile/TiO_2 nanocomposite was done by functionalizing the prepared TiO_2 on textile. Textile (1.5 g) was soaked in a solution of TiO_2 nanoparticles (150 mmol l^{-1}), with NaOH solution (7 wt%) as the solvent. The solution was stirred for 24 h and then the solution was immersed in a H_2SO_4 (5 wt%) water bath at 15 °C immediately for neutralization. After neutralization, the sample was washed with deionized water to remove the solvent. The sample was then dried in room temperature.

2.5. Synthesis of textile/Al_2O_3–TiO_2 nanocomposite

The Al_2O_3–TiO_2 bimetal oxide nanoparticles were firstly synthesized by using sol–gel method. $Al(NO_3)_3$–$9H_2O$ added to ethanol, C_2H_5OH (20 ml) and $C_6H_{10}O_3$ (ethyl acetoacetate) (30 ml) was added as a solvent. Then the solution was stirred at room temperature for 30 min. After that $C_{12}H_{28}O_4Ti$ was added to obtain a solution such that the final composition contains 30 wt% TiO_2–70 wt% Al_2O_3. Distilled water was then added to complete the hydrolysis reaction.

The solution was further stirred for 2 h and then heated at 80 °C. The obtained sample was then dried and calcined at 500 °C (2 h) and 1100 °C (2 h). The synthesis of textile/Al_2O_3–TiO_2 bimetal oxide nanocomposite was done by functionalizing Al_2O_3–TiO_2 nanoparticles on to the textile. Textile (1.5 g), Al_2O_3–TiO_2 bimetal oxide nanoparticle (150 mmol l^{-1}), and NaOH solution ((7 wt%) as the solvent) were mixed and stirred for 24 h. Then the solution was immersed in H_2SO_4 (5 wt%) water bath at 15 °C for neutralization. After neutralization, the sample was washed with deionized water to remove the solvent. The sample was then dried in room temperature.

2.6. Synthesis of textile/Al_2O_3/TiO_2 nanocomposite

Synthesis of textile/Al_2O_3/TiO_2 nanocomposite was done by functionalizing Al_2O_3 and TiO_2 nanoparticles on textile. First Al_2O_3 and TiO_2 nanoparticles were mixed physically and then the textile (1.5 g) was soaked in a solution of solution of Al_2O_3 and TiO_2 nanoparticles. The solution was then stirred for 24h and then the sample was dried in room temperature. The codes and preparation methods of the samples are given in Table 1.

2.7. Growth inhibition study

The inhibitory growth of bacteria, defined as the concentration of material that inhibits the growth of bacteria, was determined based on batch cultures containing of textile/Al_2O_3 nanocomposite, textile/Al_2O_3/TiO_2 nanocomposite (150 mmol l^{-1}) and textile/Al_2O_3–TiO_2 nanocomposite (75, 100, 125 and 150 mmol l^{-1}). Sterile side-arm Erlenmeyer flasks (250 ml) containing 50 ml of liquid broth culture (LB medium) were sonicated for 10 min after the addition of the nanocomposite to prevent aggregation. Subsequently, the flasks were inoculated with 1 ml of the freshly prepared bacterial suspension to maintain initial bacterial concentration with the role of 108 colony-forming units per millilitre, and then incubated in an orbital shaker with the speed of 200 rpm at 30 °C. The high rotary shaking speed was selected to minimize aggregation and settlement of the sample over the incubation period. Lower speed setting during incubation might cause underestimation of the antimicrobial activity of the sample. Bacterial growth was measured as the increase in absorbance at 600 nm determined using a spectrophotometer (CL-157 colorimeter; ELICO Company, Hyderabad, India). The experiments also included a positive control with a flask containing nanocomposite and nutrient medium, while the negative control was done with a flask containing textile without Al_2O_3 or TiO_2 and medium. The negative controls are used to indicate the microbial growth profile in the absence of nanocomposite. The absorbance values for positive controls were subtracted from the experimental values (flasks containing medium and nanocomposite).[26]

Table 1 Codes and preparation methods of the samples

Code	Treatment/preparation method
Al_2O_3	Sol–gel
TiO_2	Sol–gel
Al_2O_3–TiO_2	Sol–gel
Al_2O_3/TiO_2	Physical mixing
Textile/Al_2O_3	Functionalized with Al_2O_3
Textile/TiO_2	Functionalized with TiO_2
Textile/Al_2O_3–TiO_2	Functionalized with Al_2O_3–TiO_2
Textile/Al_2O_3/TiO_2	Functionalized with physically-mixed Al_2O_3/TiO_2

2.8. Characterization

The structural characterizations were performed by an X-ray diffractometer (XRD) (Bruker AXS D8 Advanced) using Cu Kα radiations ($k = 1.54178$ Å) at 40 kV and 10 mA in the range of 5–80°, scanning speed of 2 min^{-1} and resolution of 0.011. Fourier transform infrared (FTIR) spectroscopy was performed by a Nexus 670 spectrometer (Nicolet, USA) in order to identify structural features of the heat treated powders. Measurements were conducted in the wavelength range of 4000–400 cm^{-1}. All samples for FTIR measurement were mixed well with potassium bromide (KBr) in the weight ratio of 1 : 100 and then pressed into translucent pellets. A field-emission scanning electron microscope equipped with an energy dispersion X-ray spectrometer (FESEM-EDX) (JEOL JSM-6701 F) was used to observe the morphology as well as to obtain the elemental analysis of the samples. Prior to analysis, the samples were coated with gold (Au) by sputtering technique. The radical scavenging ability of the samples was measured by using a Shimadzu 1800 UV-visible spectrophotometer in the range of 250–800 nm.

2.9. Assay of scavenging activity

For the scavenging activity testing, the nanocomposites were added to the culture of *E. coli* (20 ml). The solution was shaken for 14 h at 37 °C in a shaker. The absorbances of the samples and control were determined by a UV/Vis spectrophotometer at 325 nm after 14 h. The curve was made based on the absorbance value. Scavenging activity was calculated using the following equation:[27]

$$S_a\ (\%) = \left(\frac{A_s - A_b}{A_b}\right) \times 100 \quad (1)$$

where S_a is the scavenging activity of tested sample (%), A_b is the absorbance of the control and A_s is the absorbance in the presence of the tested sample.

2.10. Metal release analysis

All samples (textile/Al_2O_3 nanocomposite, textile/TiO_2 nanocomposite, textile/Al_2O_3–TiO_2 nanocomposite and textile/Al_2O_3/TiO_2 nanocomposite and textile) were added in distilled water (20 ml) and kept 14 h, after which the nanocomposite were removed by centrifugation. The release of the inorganic content from the textile was analysed by Inductively Coupled Plasma Mass Spectrometry (ICP-MS).

2.11. Cell culture test

Human skin fibroblast, HSF (cell size of 12 μm) was cultured according to the Freshney protocol. The cells were cultured in MEM with 2 mM glutamine, 1% (v/v) PS and 10% (v/v) FBS. The attached cell cultures were maintained at specified cells concentrations of 2-9 × 10^5 cells per ml in a humidified incubator (5% CO_2 at 37 °C). A confluence stage of cell reached within 72 hour. The cells passages were used; (P11–P15). The cells were washed by PBS while the cells are about 80% confluent. They were later detached by using 0.25% trypsin/EDTA. In order to obtain cells pellets the cells were centrifuged at 2100 rpm for 5 min. The cells suspensions were used in 3 ml of MEM with a concentration of 5 × 10^5 cells per ml. Finally the cell is stained by ™Red CMTPX dye. The HSF cells in 12-well plates with or without samples were inserted into each well, 24 h before each experiment.

3. Results and discussion

3.1. Crystallinities and structure

The XRD pattern for Al_2O_3/TiO_2 nanoparticles prepared by physical mixing of TiO_2 (calcined at 800 °C) and Al_2O_3 (calcined at 1100 °C) for 2 h shown in Fig. 1(a) show mixed peaks of Al_2O_3 in the α structure and TiO_2 in the rutile form. The XRD patterns for TiO_2 (calcined at 800 °C) and Al_2O_3 (calcined at 1100 °C) are shown in Fig. 1(b) and (d), respectively. Al_2O_3 is in the α structure (corundum-like structure, where the oxygen atoms adopted hexagonal close-packing and Al^{3+} ions filling two thirds of the octahedral sites in the lattice) (ICDD 00-046-1212), while TiO_2 is in the rutile form (PDF-00-21-1276). It has been reported that the α structure of can act as radical scavenger.[28] The XRD patterns for Al_2O_3–TiO_2 nanoparticles prepared by sol–gel method and calcined at 1100 and 500 °C for 2 h are shown in Fig. 1(c) and (e), respectively. When calcination was carried out at 500 °C, the Al_2O_3–TiO_2 nanoparticles were in the amorphous phase. Calcination at 1100 °C turned the Al_2O_3–TiO_2 nanoparticles into crystalline phase.

The eight main peaks of this nanoparticle are at 2θ value of 25.78°, 35.15°, 43.35°, 52.54°, 57.49°, 61.29°, 68.21°, 77.22°, which are characterize of the α-Al_2O_3 (ICDD 00-046-1212). The peaks at around 34.45°, 48.62°, 50.07°, 59.93° are attributed to Al_2TiO_5 (PDF-18-0068), while the peaks at around 27.44°, 36.08°, 56.64°, 64.03°, 65.47° are from rutile TiO_2 (PDF-21-1276).

The crystal structure of Al_2O_3–TiO_2 bimetal oxide nanoparticles obtained in this research is different from the previously reported structure of this metal oxide,[29] which was β-Al_2TiO_5, which has a pseudobrookite crystal structure (orthorhombic lattice). In this structure, each Al^{3+} or Ti^{4+} cation is surrounded by six oxygen ions forming distorted oxygen octahedral. These AlO_6 or TiO_6 octahedral forms oriented by double chains weakly bonded by shared edges. This structural feature is responsible for the strong thermal expansion anisotropy and may induce strong antimicrobial activity.[30]

But this structure does not have any free capacity to scavenge oxygen free radicals. Therefore, although β-Al_2TiO_5 have shown antimicrobial activity (based on the oxidation ability), it cannot act as a radical scavenger.[31] Table 2 shows that the highest peak percentages came from α-Al_2O_3 while the lowest peak percentages are from Al_2TiO_5 (based on Fig. 1(C)).

3.2. Functional groups

The FTIR spectra for the samples are shown in Fig. 2. The characteristic peaks for the stretching vibrations of OH groups can be seen at about 3132–3472 cm^{-1} for all the samples which is connected to the sol–gel synthesis.[32] The hydrogen bonding between the particles of Al_2O_3–TiO_2 caused a shift in the O–H towards a higher wavenumber from 3132–3472 to 3432–3672 cm^{-1} (Fig. 2(a) and (c)). In the FTIR spectra of Al_2O_3–TiO_2 nanoparticles (Fig. 2(a)), bands due to the stretching vibrations of Al–O bonds of the octahedral coordinated Al were observed in the range of 500–750 cm^{-1}.[33] In the spectra of this sample, peaks corresponding to the Ti–O bond vibrations occur in the range of 594–639 cm^{-1}. However the FTIR spectra of textile/Al_2O_3–TiO_2 and textile/Al_2O_3/TiO_2 nanocomposites are different. This difference is caused by the bonded of TiO_2 to Al_2O_3 which result in a broader spectrum and bending of Al_2O_3 at two spectra region; 594 and 639 cm^{-1}. This band was not exhibited by textile/Al_2O_3/TiO_2 nanocomposite due to the lack of attachment of TiO_2 to Al_2O_3, which proves the difference in the structure between textile/Al_2O_3–TiO_2 and textile/Al_2O_3/TiO_2 nanocomposites. For textile/Al_2O_3–TiO_2 nanocomposite, the observed absorption peak at 639 and 694 cm^{-1} are assigned to the Al–O bonding vibrations in the Al_2O_3–TiO_2 nanoparticles, respectively (Fig. 2(a) and (c)). The broad intense bands in the range of 1200–900 cm^{-1} are attributed to cellulose, which appeared less intense in the spectra of the modified cotton (Fig. 2(c)–(f)). The presence of prominent bands at 1032 and 1059 cm^{-1} are assigned to the functional groups of cellulose,

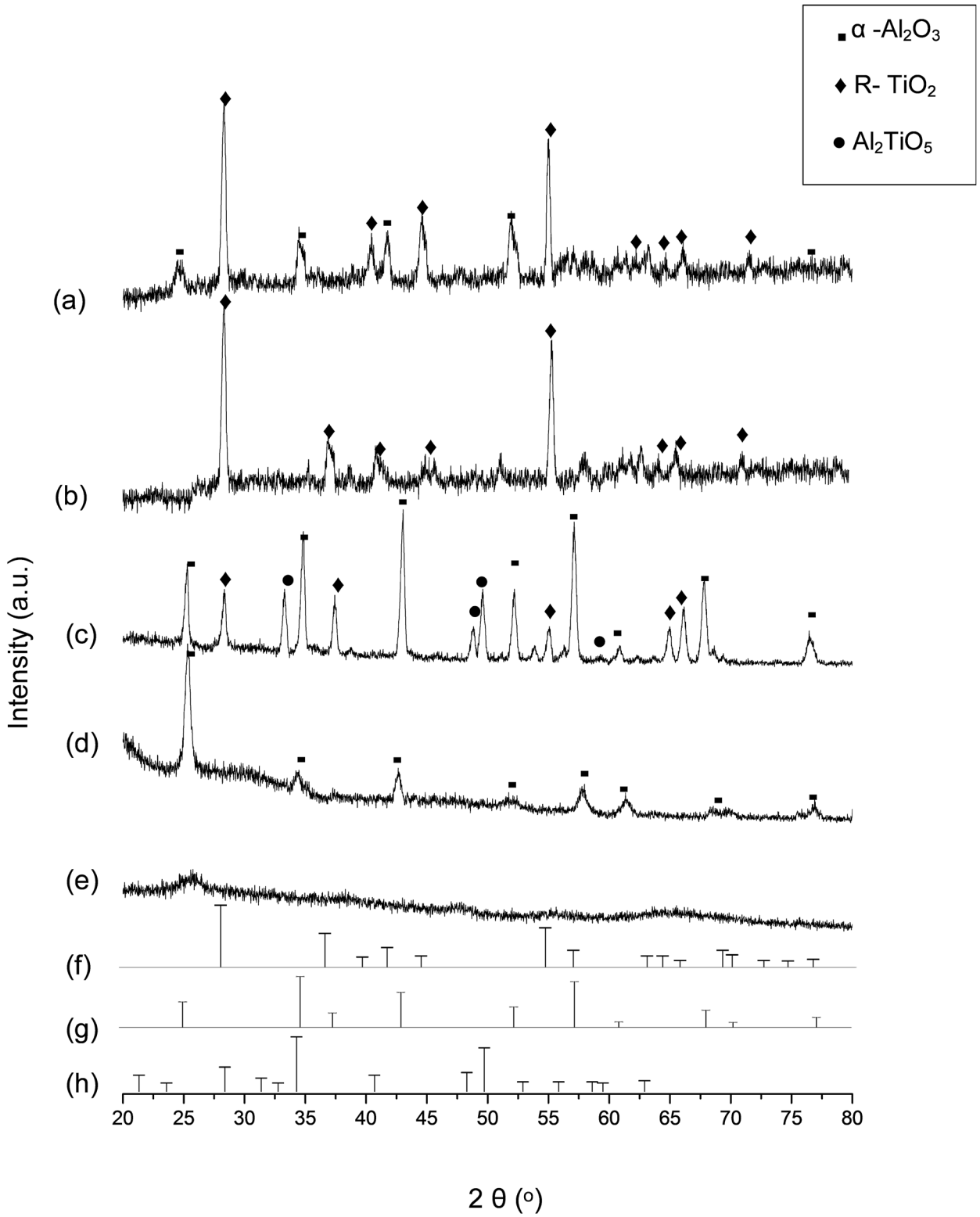

Fig. 1 XRD patterns for (a) Al_2O_3/TiO_2 (b) TiO_2 nanoparticles (c) Al_2O_3–TiO_2 nanoparticles (1100 °C) (d) Al_2O_3 nanoparticles, (e) Al_2O_3–TiO_2 nanoparticles (500 °C), (f) TiO_2 nanoparticles (PDF-21-1276), (g) Al_2O_3 (ICDD 00-046-1212), (h) Al_2TiO_5 (PDF-18-0068).

namely C–C, C–O and C–O–C stretching vibrations (Fig. 2(b)–(f)).[34] The appearance of much weaker bands around 2850–3000 cm^{-1} correspond to the C–H stretching bands, which confirms the attachment of Al_2O_3–TiO_2 nanoparticles, Al_2O_3/TiO_2 nanoparticles, Al_2O_3 nanoparticles and TiO_2 nanoparticles onto the cotton fabric (Fig. 2(c)–(f)).

Table 2 The XRD peak intensity percentage for Al_2O_3–TiO_2 nanoparticles (1100 °C)

Peak (2θ (°))	Compound	%
25.78	α-Al_2O_3	66.3
35.15	α-Al_2O_3	86.4
43.35	α-Al_2O_3	100
52.54	α-Al_2O_3	32.8
57.49	α-Al_2O_3	88.1
61.29	α-Al_2O_3	15.5
68.21	α-Al_2O_3	56.3
77.22	α-Al_2O_3	24.6
27.44	R-TiO_2	51.5
36.08	R-TiO_2	50.1
56.64	R-TiO_2	27.2
64.03	R-TiO_2	28.1
65.47	R-TiO_2	39.4
34.45	Al_2TiO_5	48.1
48.62	Al_2TiO_5	27.4
50.07	Al_2TiO_5	44.7
59.93	Al_2TiO_5	14.3

3.3. Morphology and elemental analysis

The morphology of the prepared nanocomposites observed using FESEM is shown in Fig. 3. From the figure it can be seen that the shape of the nanoparticle attached on the textile is nearly spheroidal. The EDX analysis of textile/Al_2O_3 nanocomposite and textile/Al_2O_3–TiO_2 nanocomposite are shown in Fig. 4. Based on the EDX analysis, there are four main elements in textile/Al_2O_3 nanocomposite. The elements are carbon (C), aluminium (Al), oxygen (O) and Au (the coating material), with focus on Al and O. The EDX analysis of textile/Al_2O_3–TiO_2 nanocomposite shows five elements, which are Al, Ti, C, O and Au (the coating material). The EDX analysis also shows Al, Ti and O in textile/Al_2O_3–TiO_2 nanocomposite. Based on the FESEM image and EDX analysis, it can be concluded that the textile/Al_2O_3 nanocomposite and Al_2O_3–TiO_2/textile nanocomposite were successfully obtained. Based on Fig. 5 the size of the Al_2O_3–TiO_2 particles attached on the textile were in the range of 50–80 nm, which confirms that these particles are in the nano range.

The FESEM image and EDX analysis of textile/Al_2O_3–TiO_2 nanocomposite and textile/Al_2O_3/TiO_2 nanocomposite are shown in Fig. 3(d), 4(c), 3(e) and 4(e). As for the EDX analysis of textile/TiO_2 nanocomposite, three elements (Ti, O, and C) can be seen in this nanocomposite. Finally, The FESEM images shown in Fig. 3(b)–(e) display the presence of attachment on the cotton textile after modification. The inset of Fig. 3(b)–(e) show the appearance of frequent roughness and wrinkles on the textiles' surface, verifying the successful attachment of these nanoparticles onto the cotton textile. The robust surface roughness of textile/Al_2O_3 nanocomposite, textile/TiO_2 nanocomposite, textile/Al_2O_3–TiO_2 nanocomposite and textile/Al_2O_3/TiO_2 nanocomposite are presented in Fig. 3(b)–(e) are due to the

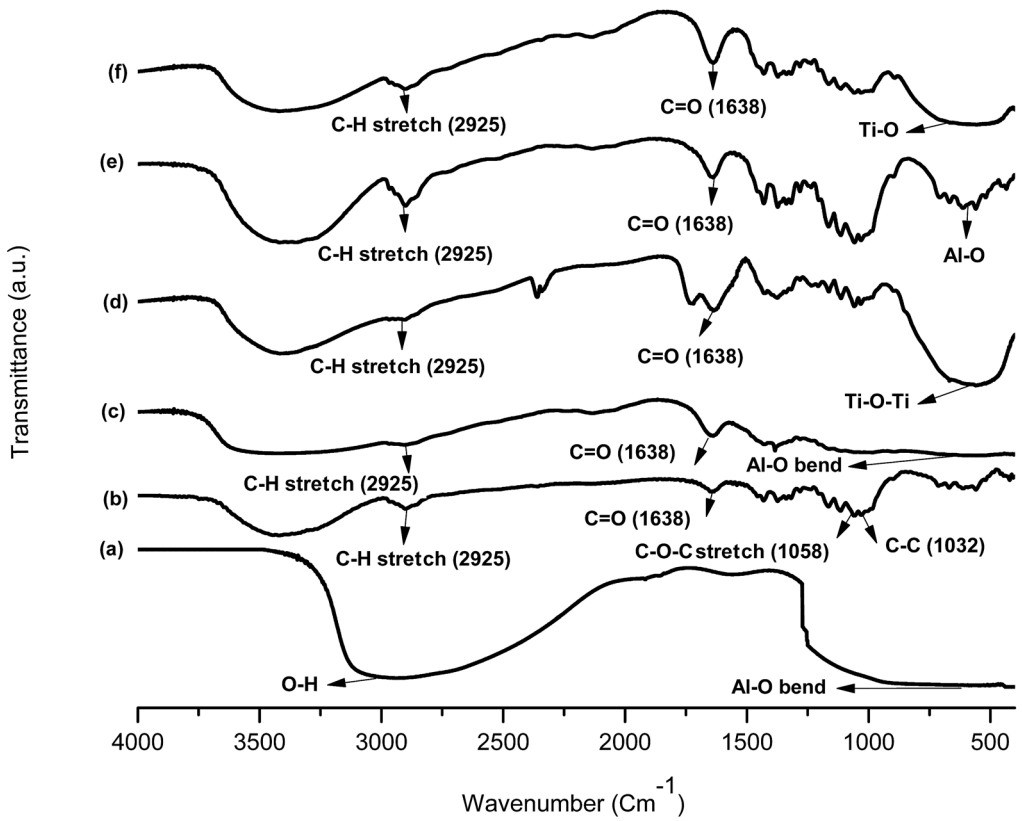

Fig. 2 FTIR spectra of (a) Al_2O_3–TiO_2 nanoparticles, (b) textile, (c) textile/Al_2O_3–TiO_2/textile nanocomposite, (d) textile/Al_2O_3/TiO_2 nanocomposite, (e) textile/Al_2O_3 nanocomposite and (f) textile/TiO_2 nanocomposite.

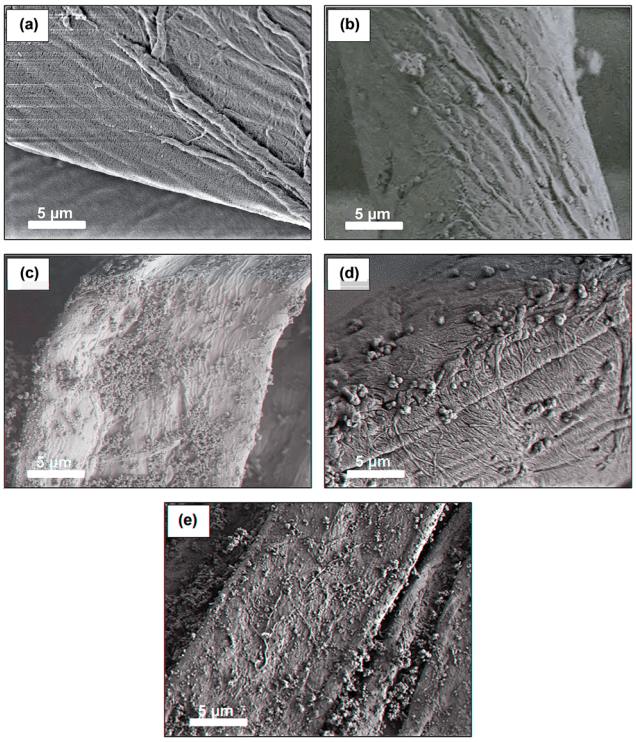

Fig. 3 FESEM images of (a) textile, (b) textile/Al_2O_3 nanocomposite, (c) textile/TiO_2 nanocomposite, (d) textile/Al_2O_3–TiO_2 nanocomposite, (e) textile/Al_2O_3/TiO_2 nanocomposite.

growth of nearly spherical nanoparticles on the surface of cotton textile. The inset of Fig. 3(b)–(e) clearly reveal the attachment of these nearly spherical nanoparticles.

From the combination of these results with FTIR results, it can be concluded that this attachment is accrued by the hydrogen bonding between the O–H of the nanoparticles and the O–H of the textiles' surface. This attachment is nearly stable because these nanocomposites washability by distilled water after modification, and the low release of metal oxide from these textile nanocomposites also confirm the stability of this attachment.

3.4. Antimicrobial ability

For antimicrobial ability testing, strains of Gram-negative bacterium *E. coli* were inoculated in LB medium supplemented with increasing dosages of textile/Al_2O_3–TiO_2 nanocomposite in different concentrations (150, 125, 100 and 75 mmol l^{-1}). Increasing concentration of the nanoparticles progressively retarded the growth of *E. coli* (Fig. 6). The concentration of 150 mg ml^{-1} of textile/Al_2O_3–TiO_2 nanocomposite was found to be strongly inhibitory for bacteria. The steepness of the growth curve in the logarithmic phase and the final cell concentration were also noticeably lower at the concentration of 125 and 150 mmol l^{-1}, as compared with the lower concentrated ones used in this study (75 and 100 mmol l^{-1}). The antimicrobial ability comparison between textile/Al_2O_3 nanocomposite, textile/TiO_2 nanocomposite, textile/Al_2O_3–TiO_2 nanocomposite, textile/Al_2O_3/TiO_2 nanocomposite, textile and

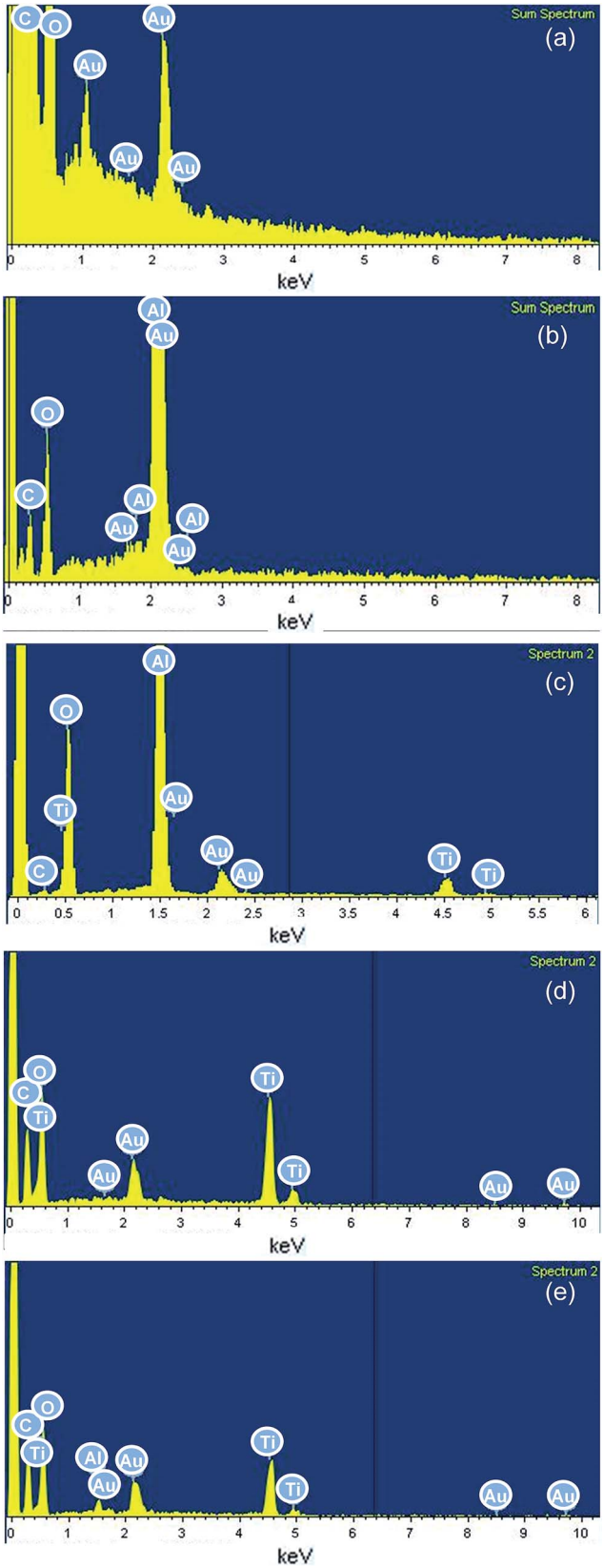

Fig. 4 EDX analysis of (a) textile, (b) textile/Al_2O_3 nanocomposite, (c) textile/Al_2O_3–TiO_2 nanocomposite, (d) textile/TiO_2 nanocomposite, (e) textile/Al_2O_3/TiO_2 nanocomposite.

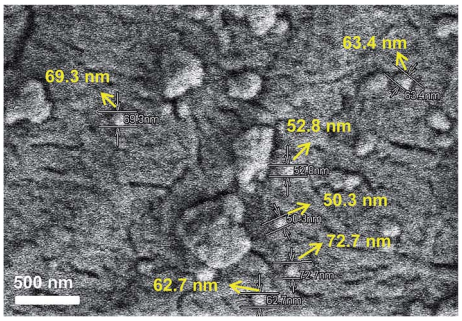

Fig. 5 The particle size of textile/Al_2O_3–TiO_2 nanocomposite measured from FESEM image.

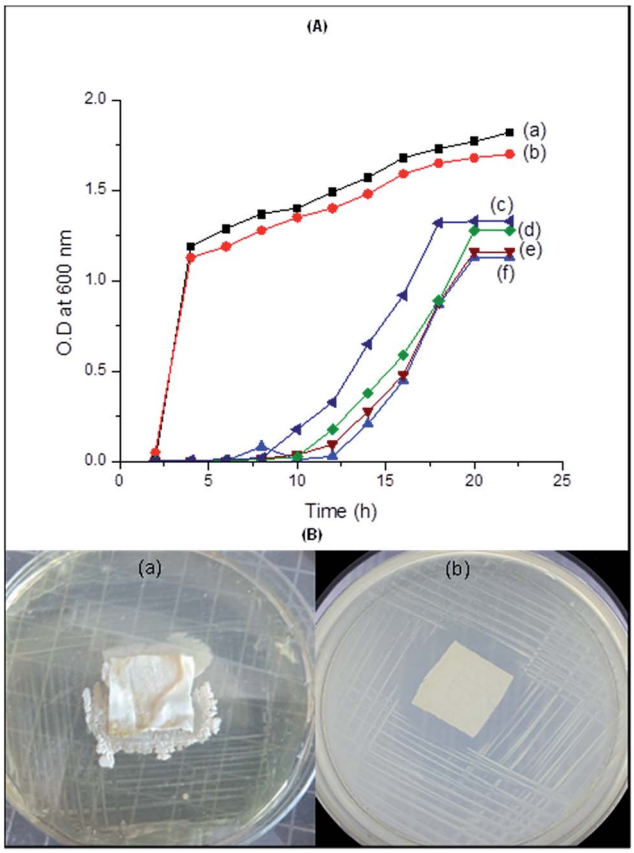

Fig. 6 Growth of *E. coli* against textile/Al_2O_3–TiO_2 nanocomposite in different concentrations (150, 125, 100 and 75 mmol l^{-1}) in (A) liquid medium (LB) (a) culture (b) textile (c) 75 mmol l^{-1} (d) 100 mmol l^{-1} (e) 125 mmol l^{-1} (f) 150 mmol l^{-1} and (B) agar medium (a) textile (b) textile/Al_2O_3–TiO_2 nanocomposite.

culture after 14 h is shown in Fig. 7. Textile/Al_2O_3 nanocomposite shows mild inhibitory against *E. coli*, even when high concentration (150 mmol l^{-1}) was used.

On the other hand, the antimicrobial ability of textile/Al_2O_3–TiO_2 nanocomposite was much higher than those shown by textile/TiO_2 nanocomposite and textile/Al_2O_3/TiO_2 nanocomposite. Antimicrobial ability has reverse link with bacteria growth therefore, the comparison trend between all samples after 14 h based on Fig. 7 is as follows: textile/Al_2O_3–TiO_2

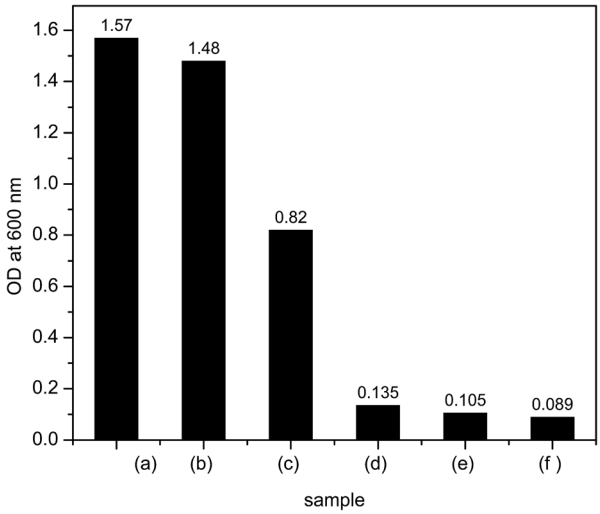

Fig. 7 Growth *E. coli* after 14 h shown by: (a) culture, (b) textile, (c) textile/Al_2O_3 nanocomposite, (d) textile/TiO_2 nanocomposite, (e) textile/Al_2O_3/TiO_2 nanocomposite and (f) textile/Al_2O_3–TiO_2 nanocomposite.

nanocomposite > textile/Al_2O_3/TiO_2 nanocomposite > textile/TiO_2 nanocomposite > textile/Al_2O_3 nanocomposite > textile > culture. The antimicrobial ability of nanoparticles is also related to the size of the nanoparticles.[15,17] Smaller-sized nanoparticles have better antimicrobial ability as they possess large surface area. As antibacterial activity is known as the function of the surface area in contact with the microorganisms, therefore, a larger surface area (as in the case of nanoparticles) shows a broader range of probable reactions with bioorganic present on the cell surface.[15] The particle size of Al_2O_3–TiO_2 nanoparticles attached to textile is around 50–80 nm (Fig. 5). This nanocomposite shows higher antimicrobial activity compared to textile/Al_2O_3 nanocomposite because of the presence of TiO_2 in the structure of Al_2O_3–TiO_2 nanoparticles, which caused the increase in antimicrobial activity of this nanocomposite. The strong bactericidal effect, as observed with some metal oxides such as TiO_2, was not observed in the case of Al_2O_3.[35]

The disruption of cell wall due to the generation of ROS is one of the most important mechanisms behind cell death leading to the strong antimicrobial property of these metal oxides. ROS is very toxic to human body. Consequently, it is evident from this study that Al_2O_3–TiO_2 nanoparticles on textile possess strong antimicrobial properties; high growth inhibition was noticed at high concentration of nanoparticles of up to 100 mmol l^{-1}. These observations are pertinent to the ecotoxicity of textile/Al_2O_3–TiO_2 nanocomposite against bacteria. This laboratory-scale study suggests that textile/Al_2O_3–TiO_2 is strongly toxic to microorganisms in the environment.

3.5. Radical scavenging ability

The amount of radical scavenging ability of textile/Al_2O_3 nanocomposite, textile/Al_2O_3/TiO_2 nanocomposite, textile/Al_2O_3–TiO_2 nanocomposite, textile/TiO_2 nanocomposite and textile as the control is calculated by eqn (1) and shown in Table 3.

Table 3 Radical scavenging ability of textile/TiO_2, textile/Al_2O_3 nanocomposite, textile/Al_2O_3/TiO_2 nanocomposite and textile/Al_2O_3–TiO_2 nanocomposite

Samples	Absorbance of the samples (A_s)	Radical scavenging ability (%S_a)
Textile/Al_2O_3–TiO_2 nanocomposite	0.623	38.2%
Textile/Al_2O_3/TiO_2 nanocomposite	0.654	35.5%
Textile/Al_2O_3 nanocomposite	0.660	35.0%
Textile/TiO_2 nanocomposite	1.015	0.2%

The comparison of radical scavenging ability between negative and positive samples is also reported in Table 3. Based on the Table 3, textile/Al_2O_3–TiO_2 nanocomposite has the highest radical scavenging ability (38.2%), due to the structure of this nanocomposite. The radical scavenging ability of textile/Al_2O_3 nanocomposite and textile/Al_2O_3/TiO_2 nanocomposite are 35 and 35.5%, respectively. Although textile/TiO_2 nanocomposite has strong antimicrobial ability, it did not show any radical scavenging ability. On the other hand, textile/Al_2O_3–TiO_2 nanocomposite has shown high radical scavenging ability.

3.6. Cytotoxicity

The fluorescent microscopy image of human skin fibroblasts (HSF) growth on the treatment of all samples, 2 days post seeding can be seen in Fig. 8, respectively. For both textile/Al_2O_3 nanocomposite and textile/Al_2O_3–TiO_2 nanocomposite, the cell culture indicates improved cell viability and proliferation. No discernible difference can be seen between these two types of textile nanocomposite. This result confirms the radical scavenger ability of these nanocomposites. In the case of textile/Al_2O_3/TiO_2 nanocomposite, the cell culture shows cell viability lower than previous nanocomposite. On the other hand textile/TiO_2 nanocomposite does not show any cell viability because it cannot act as radical scavenger and ROS could have been be distributed through the cell wall of HSF.

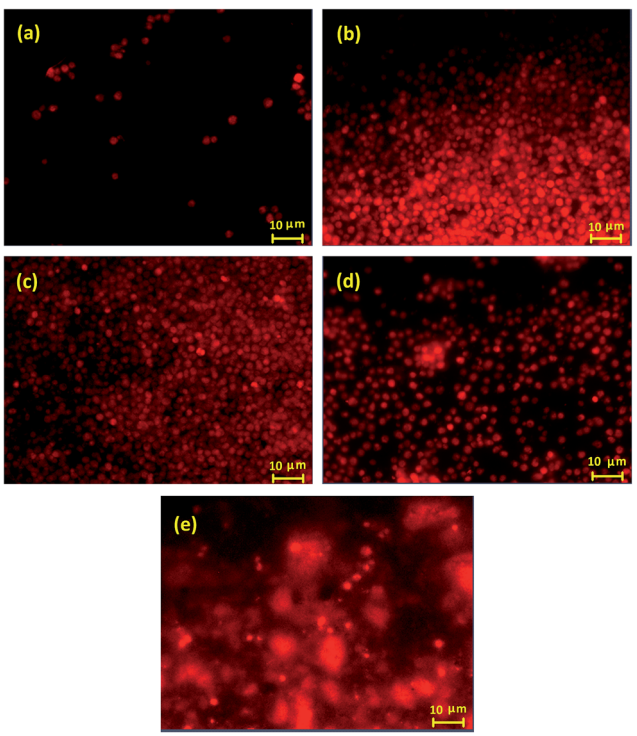

Fig. 8 The fluorescent microscopy image of human skin fibroblasts (HSF) growth on the different treatment: (a) without treatment, (b) textile/Al_2O_3 nanocomposite, (c) textile/Al_2O_3–TiO_2 nanocomposite, (d) textile/Al_2O_3/TiO_2 nanocomposite, (e) textile/TiO_2 nanocomposite.

Table 4 The release of the inorganic content from the textile of textile/Al_2O_3 nanocomposite, textile/Al_2O_3/TiO_2 nanocomposite, textile/Al_2O_3–TiO_2 nanocomposite, textile/TiO_2 nanocomposite

Samples	Inorganic release amount (μg l^{-1})
Textile/Al_2O_3–TiO_2 nanocomposite	9.831
Textile/Al_2O_3/TiO_2 nanocomposite	14.071
Textile/Al_2O_3 nanocomposite	7.160
Textile/TiO_2 nanocomposite	11.340

The release of the inorganic content from the textile of textile/Al_2O_3 nanocomposite, textile/Al_2O_3/TiO_2 nanocomposite, textile/Al_2O_3–TiO_2 nanocomposite, textile/TiO_2 nanocomposite is shown in Table 4. Based on Table 4, textile/Al_2O_3–TiO_2 nanocomposite and textile/Al_2O_3 have the lowest amount of inorganic release from textile. Therefore, the attachment of these nanoparticles of textile is almost stable.

The application of surface modification of textile is an accepted technique to improve the initial antimicrobial, radical scavenger and biocompatibility of textile/Al_2O_3–TiO_2 nanocomposite. Al_2O_3–TiO_2 nanoparticles can be used to provide localized high wound healing to the textile. With the intention to increase both antimicrobial ability and nontoxicity of biological agents, the textile/Al_2O_3–TiO_2 nanocomposite is suggested to be used as wound dressing. This antimicrobial and non-toxic wound dressing can improve wound healing process.

4. Conclusions

Textile/Al_2O_3 nanocomposite, textile/Al_2O_3/TiO_2 nanocomposite, textile/TiO_2 nanocomposite and textile/Al_2O_3–TiO_2 nanocomposite were successfully synthesized *via* the sol–gel method and attachment on textile. The role of Al_2O_3–TiO_2 in antimicrobial and radical scavenging properties was studied through in-depth characterizations at room temperature. The presence of TiO_2 in Al_2O_3–TiO_2 nanoparticles is found to increase the antimicrobial ability of textile/Al_2O_3–TiO_2 nanocomposite. The textile/Al_2O_3–TiO_2 nanocomposite shows strong antimicrobial activity and the ability to scavenge ROS. The outstanding features of the results indicate that this easy and environmental-friendly preparation method can be used as an effective wound dressing.

Acknowledgements

The authors gratefully acknowledge funding from Universiti Teknologi Malaysia (UTM) through Research University Grant.

D. H. B. Wicaksono acknowledges funding from RU Grant 05H32. H. Nur acknowledges funding from the Ministry of Education (MOE) under FRGS grant no. FRGS/2/2014/SG06/UTM/01/1. The authors also would like to thank Prof. Dr Fahrul Zaman Huyop (Faculty of Biosciences and Medical Engineering, UTM) for his support in the antimicrobial analysis.

References

1 H. Kim, I. Makin, J. Skiba, A. Ho, G. Housler, A. Stojadinovic and M. Izadjoo, *Open Microbiol. J.*, 2014, **8**, 15–21.
2 J. Banerjee, P. D. Ghatak, S. Roy, S. Khanna, E. K. Sequi, K. Bellman, B. C. Dickinson, P. Suri, V. V. Subramaniam, C. J. Chang and C. K. Sen, *PLoS One*, 2014, **9**, e89239.
3 R. Jayakumar, M. Prabaharan, P. S. Kumar, S. Nair and H. Tamura, *Biotechnol. Adv.*, 2011, **29**, 322–337.
4 C. K. Bower, J. E. Parker, A. Z. Higgins, M. E. Oest, J. T. Wilson, B. A. Valentine, M. K. Bothwell and J. McGuire, *Colloids Surf., B*, 2002, **25**, 81–90.
5 S. J. Soenen, P. Rivera-Gil, J.-M. Montenegro, W. J. Parak, S. C. De Smedt and K. Braeckmans, *Nano Today*, 2011, **6**, 446–465.
6 L. Yildirimer, N. T. K. Thanh, M. Loizidou and A. M. Seifalian, *Nano Today*, 2011, **6**, 585–607.
7 X. Ren, L. Kou, H. B. Kocer, C. Zhu, S. Worley, R. Broughton and T. Huang, *Colloids Surf., A*, 2008, **317**, 711–716.
8 P. Kaushik and A. Malik, *Environ. Int.*, 2009, **35**, 127–141.
9 J. V. Edwards and T. L. Vigo, *Bioactive fibers and polymers*, Oxford University Press, 2001.
10 C. G. Gebelein and C. E. Carraher, *Biotechnology and bioactive polymers*, Springer, 1994.
11 M. Montazer and M. G. Afjeh, *J. Appl. Polym. Sci.*, 2007, **103**, 178–185.
12 R. Dastjerdi, M. Mojtahedi, A. Shoshtari and A. Khosroshahi, *J. Text. Inst.*, 2010, **101**, 204–213.
13 N. Ladhari, M. Baouab, A. Ben Dekhil, A. Bakhrouf and P. Niquette, *J. Text. Inst.*, 2007, **98**, 209–218.
14 J. M. Miller and L. J. Lakshmi, *J. Phys. Chem. B*, 1998, **102**, 6465–6470.
15 H. Gleiter, *Acta Mater.*, 2000, **48**, 1–29.
16 A. Curtis and C. Wilkinson, *Trends Biotechnol.*, 2001, **19**, 97–101.
17 X. Qiu, M. Miyauchi, K. Sunada, M. Minoshima, M. Liu, Y. Lu, D. Li, Y. Shimodaira, Y. Hosogi, Y. Kuroda and K. Hashimoto, *ACS Nano*, 2012, **6**, 1609–1618.
18 S. Makhluf, R. Dror, Y. Nitzan, Y. Abramovich, R. Jelinek and A. Gedanken, *Adv. Funct. Mater.*, 2005, **15**, 1708–1715.
19 P. Holister, J. W. Weener, V. C. Romas and T. Harper, *Nanoparticles: technology white papers 3*, Scientific Ltd, 2003.
20 R. Brayner, R. Ferrari-Iliou, N. Brivois, S. Djediat, M. F. Benedetti and F. Fiévet, *Nano Lett.*, 2006, **6**, 866–870.
21 P. ZielińAski, R. Schulz, S. Kaliaguine and A. Van Neste, *J. Mater. Res.*, 1993, **8**, 2985–2992.
22 P. Ganguly and W. J. Poole, *Mater. Sci. Eng., A*, 2003, **352**, 46–54.
23 R. Dastjerdi and M. Montazer, *Colloids Surf., B*, 2010, **79**, 5.
24 A. Nilghaz, D. H. Wicaksono, D. Gustiono, F. A. A. Majid, E. Supriyanto and M. R. A. Kadir, *Lab Chip*, 2012, **12**, 209–218.
25 J. Li, Y. Pan, C. Xiang, Q. Ge and J. Guo, *Ceram. Int.*, 2006, **32**, 587–591.
26 D. N. Williams, S. H. Ehrman and T. R. P. Holoman, *J. Nanobiotechnol.*, 2006, **4**, 3.
27 Z. Yaping, Y. Wenli, W. Dapu, L. Xiaofeng and H. Tianxi, *Food Chem.*, 2003, **80**, 115–118.
28 G. Mohammad, V. K. Mishra and H. Pandey, *Digest Journal of Nanomaterials and Biostructure*, 2008, **3**, 159–162.
29 S. Hoffmann, S. T. Norberg and M. Yoshimura, *J. Electroceram.*, 2006, **16**, 327–330.
30 R. W. Grimes and J. Pilling, *J. Mater. Sci.*, 1994, **29**, 2245–2249.
31 H. Bian, Y. Yang, Y. Wang, W. Tian, H. Jiang, Z. Hu and W. Yu, *J. Mater. Sci. Technol.*, 2013, **29**, 429–433.
32 W. Mozgawa, M. Król and T. Bajda, *J. Mol. Struct.*, 2009, **924**, 427–433.
33 P. Padmaja, G. Anilkumar, P. Mukundan, G. Aruldhas and K. Warrier, *Int. J. Inorg. Mater.*, 2001, **3**, 693–698.
34 K. Kavkler, N. Gunde-Cimerman, P. Zalar and A. Demšar, *Polym. Degrad. Stab.*, 2011, **96**, 574–580.
35 A. Besinis, T. De Peralta and R. D. Handy, *Nanotoxicology*, 2014, **8**, 1–16.